Phys Chem Minerals (2003) 30: 582–588
DOI 10.1007/s00269-003-0351-1

ORIGINAL PAPER

H. Liu · W. A. Caldwell · L. R. Benedetti
W. Panero · R. Jeanloz

Static compression of α-Fe_2O_3: linear incompressibility of lattice parameters and high-pressure transformations

Received: 3 January 2003 / Accepted: 1 July 2003

Abstract The high-pressure behavior of α-Fe_2O_3 has been studied under static compression up to 60 GPa, using a laser-heated diamond anvil cell. Synchrotron-based angular-dispersive X-ray diffraction shows that the sample remains in the corundum structure up to 50 GPa, but with the appearance of coexisting diffraction lines from a high-pressure phase at pressures above 45 GPa. A least-squares fit of low-pressure phase data to an Eulerian finite-strain equation of state yields linear incompressibilities of $K_{a0} = 749.5$ ($\pm$ 18.4) GPa and $K_{c0} =$ 455.7 ($\pm$ 21.4) GPa, differing by a factor of 1.6 along the two directions. The enhanced compressibility of the *c* axis may lead to breaking of vertex- or edge-sharing bonds between octahedra, inducing the high-pressure phase transformation at 50 GPa. Analysis of linear compressibilities suggests that the high-pressure phase above 50 GPa is of the Rh_2O_3 (II) structure. Continuous laser heating reveals a new structural phase transformation of α-Fe_2O_3 at 22 GPa, to an orthorhombic structure with a = 7.305(3) Å, b = 7.850(3) Å, and c = 12.877(14) Å, different from the Rh_2O_3 (II) structure.

Keywords α-Fe_2O_3 · High pressure · Linear compressibility · Synchrotron X-ray diffraction · Rh_2O_3 (II)-type structure

Introduction

The high-pressure behavior of α-Fe_2O_3, an important end-member compound for characterizing the properties of trivalent iron (Fe^{3+}) in the Earth's mantle, has been of long-standing interest to geophysics. Evidence of a high-pressure phase transformation in α-Fe_2O_3 was first observed in shock-wave experiments at pressures above 50 GPa (McQueen and Marsh 1966), and subsequently documented by static compression using diamond-anvil cells (Yagi and Akimoto 1982; Suzuki et al. 1985; Knittle and Jeanloz 1986; Olsen et al. 1991). There has been controversy regarding the structure of the high-pressure phase (Reid and Ringwood 1969; Pasternak et al. 1999). Some authors proposed the transition to be from corundum to $GdFeO_3$-type orthorhombic perovskite structures (Reid and Ringwood 1969; Olsen et al. 1991), whereas other authors prefer the Rh_2O_3(II)-type structure that has been documented as a high-pressure phase of Rh_2O_3 (Shannon and Prewitt 1970).

It has generally not been possible to differentiate between the $GdFeO_3$-type orthorhombic perovskite and the Rh_2O_3(II) structures based on measured X-ray diffraction data, however. Other experimental measurements and theoretical calculations have therefore been invoked to clarify the nature of this transition. Early Mössbauer measurements at high pressure and 300 K (Syono et al. 1984; Suzuki et al. 1985) revealed a nonmagnetic component at ~50 GPa, coexisting with a magnetic phase to a pressure of at least 70 GPa. The interpretation that the high-pressure phase of Fe_2O_3 is characterized by two kinds of iron ions with different crystallographic sites suggested that the high-pressure phase has the $GdFeO_3$ orthorhombic perovskite structure. On the other hand, ab initio calculations (Cynn et al. 1990; Marton and Cohen 1994; Thomson et al. 1996) predicted that the structural analogue Al_2O_3 transforms from the corundum structure to the Rh_2O_3(II) structure at high pressures, and this was subsequently confirmed with laser-heated diamond-cell experiments (Funamori and Jeanloz 1997).

More recently, Pasternak et al. (1999) reported new measurements of Mössbauer spectra and electrical resistance of Fe_2O_3 to pressure over 80 GPa. They obtained a pure high-pressure component of Fe_2O_3, and assigned it to a nonmagnetic and metallic phase in which there is only one iron site. By comparative analysis of the observed

H. Liu · W. A. Caldwell · W. Panero · R. Jeanloz (✉)
Department of Earth and Planetary Science,
University of California, Berkeley, California 94720, USA
e-mail: jeanloz@uclink.berkeley.edu
Tel: +1-510-642-2639
Fax: +1-643-9980

L. R. Benedetti
Department of Physics, University of California,
Berkeley, California 94720, USA

O–O bond lengths, the new Mössbauer spectroscopy results, and ab initio calculations, this high-pressure phase was assigned to the Rh_2O_3(II) structure (Rozenberg et al. 2002). Some aspects of their interpretation have been challenged by Badro et al. (2002), however.

Here, we present new static-compression results for α-Fe_2O_3 as it crosses over into the high-pressure phase, analyzing its detailed elastic properties in order to clarify the nature of the high-pressure structure.

Experimental

The starting material used in the present study is α-Fe_2O_3 of 99.9% purity obtained from Alfa Chemicals. Samples are loaded into a gasketed Mao–Bell-type diamond-anvil cell, using diamonds with 350-μm diameter culets and a pre-indented metal gasket. A rhenium gasket with 150-μm hole is used along with argon as a pressure medium. The gasket squeezes around the edges of the diamond to provide additional support at the culet edge, to minimize pressure gradients across the sample, and to allow the enclosure of hydrostatic and quasihydrostatic media between the diamonds. All samples are gasketted, but in the present study some were loaded without an argon pressure medium in order to investigate the effects of shear stresses on the results.

Samples were laser-heated using the 1064-nm radiation from a Quantronix 117 Nd-YAG laser with 100 W (multimode) CW power. The thermal radiation emitted from the sample during laser heating is recorded over the wavelength range 400–900 nm using an imaging spectrograph and a EG&G PARC Model 1430-P charged-couple device (CCD) detector. Temperatures are then obtained using an inverse Abel transform combined with a graybody fit to the intensity of thermal radiation (Jeanloz and Heinz 1984; Heinz and Jeanloz 1987; Jeanloz and Kavner 1996).

X-ray diffraction patterns were collected at high pressure and room temperature by synchrotron-based angular-dispersive X-ray diffraction at the Stanford Synchrotron Radiation Laboratory (SSRL), beamline 10-2. X-rays from the synchrotron source are monochromatized by a single-crystal monochromator [Si (111)] at an energy of 17.038 keV (corresponding to $\lambda = 0.7277$ Å). Between the incident beam and the sample, a pinhole collimator (1 mm entry diameter and 60–750 μm exit diameter) is used to adjust the beam size. Diffracted X-rays are recorded on an imaging plate (20 × 40 cm) placed behind the diamond-anvil cell, and the diffraction data were analyzed by integrating the recorded patterns (Ngyuen and Jeanloz 1993). The lattice parameters and unit-cell volume for hematite were then determined at each pressure from six to nine diffraction lines: (012), (104), (110), (113), (024), (116), and (018), (214), (300). Pressures were determined by ruby fluorescence, or calculated from argon diffraction lines using the equation of state of argon (Ross et al. 1986).

Results and discussion

Static compression without laser heating

X-ray diffraction patterns for α-Fe_2O_3, with or without a pressure medium, are summarized in Fig. 1. The observed *d*-spacings versus pressure are plotted in Fig. 2, and it can be seen that a high-pressure phase transition occurs around 50 GPa for both sets of measurements. More detail comes from the quasihydrostatic measurement (Fig. 1a): evidence of a high-pressure phase first appears by 47 GPa, new diffraction lines emerge with increasing pressure and the transition is complete by 53 GPa. This is in good agreement with the results of previous studies (Suzuki et al. 1985; Knittle and Jeanloz 1986; Olsen et al. 1991). The high-pressure phase transition is reversible, and the crystal structure reverts to that of hematite upon decompression. Comparing with previous results, our diffraction patterns complement the information provided by Suzuki et al. (1985) and Olsen et al. (1991): all reveal the same high-pressure transformation, and here we present the diffraction patterns obtained for the high-pressure phase.

From the measured X-ray diffraction patterns, we calculate the pressure dependence of the lattice parameters, *a* and *c*, for hematite (low-pressure phase) as summarized in Table 1 and Fig. 3. The *c* axis shows a linear compression over the entire pressure range of our

Fig. 1a, b Selected X-ray diffraction patterns of α-Fe_2O_3 under static compression: *LP* denotes the low-pressure phase (corundum structure) and *HP* the high-pressure phase (Rh_2O_3 (II) structure). **a** With argon as pressure medium (SSRL3/99). The diffraction lines of the high-pressure phase begin to appear at 46.9 GPa, and the transformation is complete by about 52.8 GPa. **b** Without pressure medium (SSRL11/97). The sample remains in the hematite structure up to 41.2 GPa, the high-pressure phase transformation is complete by about 53.6 GPa, and the sample reverts to hematite (corundum structure) upon decompression

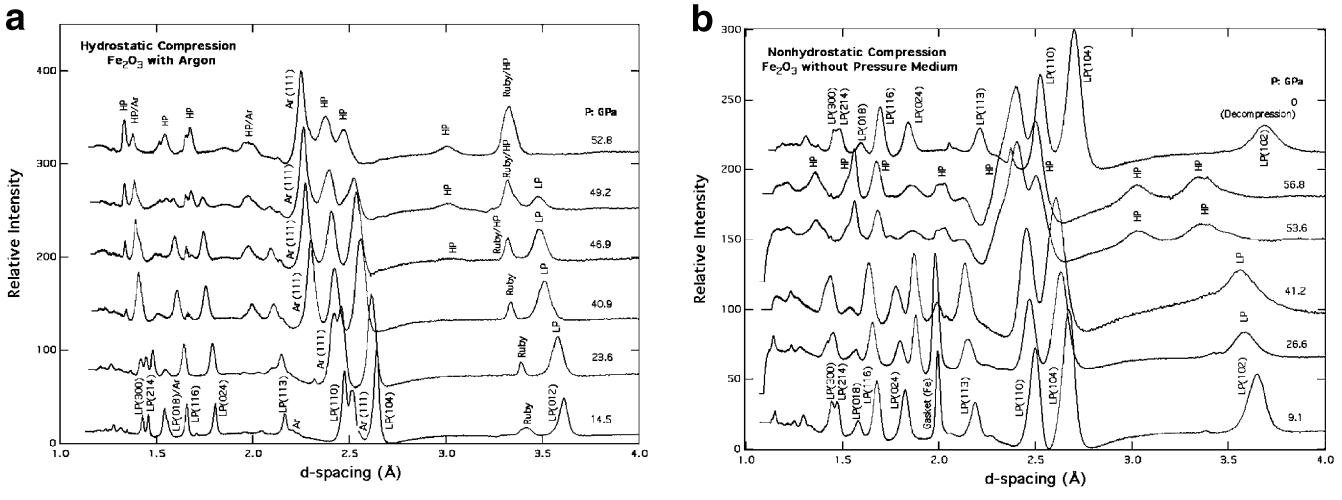

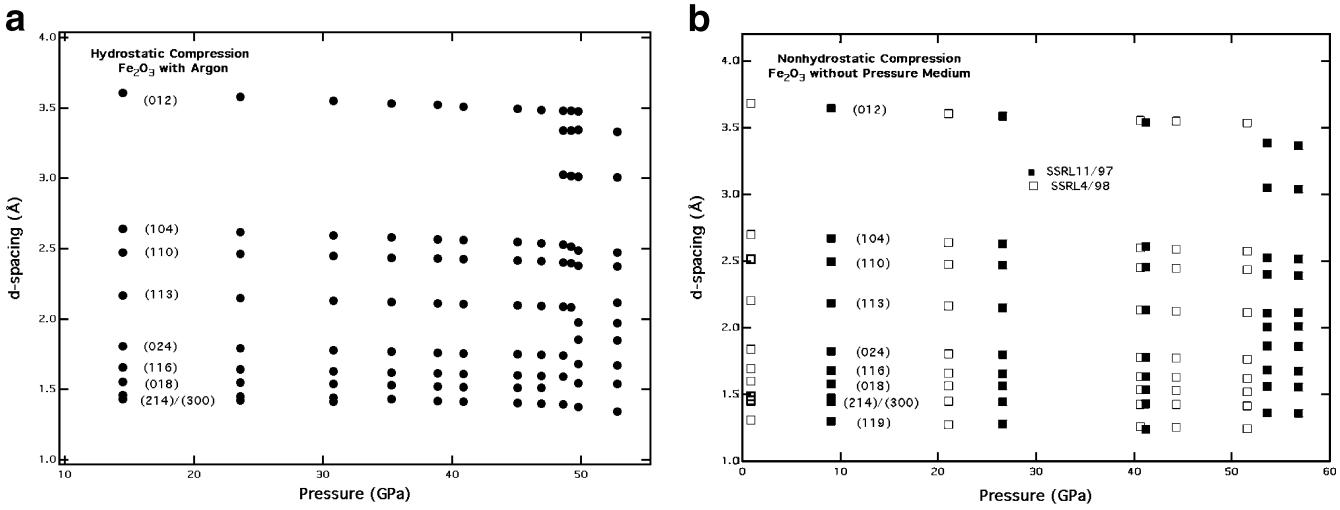

Fig. 2a, b Measured *d*-spacings versus pressure for α-Fe_2O_3 under static compression. **a** With argon as pressure medium (SSRL3/99), showing the high-pressure phase transition beginning at 46.9 GPa. **b** Without pressure medium, showing the high-pressure phase above 50 GPa. Data are taken from two different runs: *solid squares* from run SSRL11/97, *open squares* from run SSRL4/98

experiment; the *a* axis also decreases linearly with pressure, but with an apparent deviation from linearity above 45 GPa at which the structural transition begins. The ratio of c/a decreases from 2.731 ($\pm$ 0.002) at zero pressure to 2.657 ($\pm$ 0.002) at 48.6 GPa, indicating different compressibilities along the two different crystallographic directions.

Bulk modulus and linear incompressibility

X-ray diffraction measurements allow us to determine the bulk modulus and elastic properties using the Birch–Murnaghan equation of state (Birch 1978):

$$P = 3K_0 f_v (1 + 2f_v)^{5/2}[1 + af_v + bf_v^2 + \ldots] \ , \qquad (1)$$

where $f_v = 1/2[(V_0/V)^{2/3} - 1]$ is the volumetric Eulerian finite-strain measure, K_0 is the bulk modulus at zero-pressure and room temperature, and $a = 3(K_0' - 4)/2$ is the third-order coefficient of energy in strain f_v(K_0' is the derivative of K_0 with respect to pressure).

It is well known that $K_0' = 4$ is suitable for most materials, implying that a second-order equation of state is often valid for analyzing equation-of-state measurements (Birch 1978; Jeanloz 1989). Applying Eq. (1) to the hydrostatic compression *P–V* data in Table 1, and assuming $K_0' = 4$, we obtain a zero-pressure bulk modulus $K_0' = 206.1$ ($\pm$ 4.8) GPa from a weighted fit to the measurements. This value is in good agreement with the ultrasonically determined isothermal modulus, $K_{T0} = 202.7$ GPa (Liebermann and Schreiber 1968). A weighted fit to the third-order equation of state gives $K_0 = 202.1$ ($\pm$ 3.8) GPa and $K_0' = 4.3$ ($\pm$ 0.3),

Table 1 X-ray diffraction results for α-Fe_2O_3 low-pressure phase

Run no.	P (GPa)	*a* (Å)	*c* (Å)	*V* (Å)	*c*/*a*	Note
ssrl3/99	9.1(1)	4.971(1)	13.497(5)	48.13(3)	2.715(1)	Hydrostatic[a]
	14.5(3)	4.947(1)	13.398(5)	47.31(3)	2.708(1)	
	23.6(4)	4.917(4)	13.24(2)	46.19(9)	2.693(5)	
	30.8(8)	4.889(4)	13.09(2)	45.1(1)	2.677(5)	
	35.3(6)	4.863(4)	13.03(2)	44.5(1)	2.679(5)	
	38.9(6)	4.850(4)	12.95(2)	43.9(1)	2.670(5)	
	40.9(6)	4.840(6)	12.90(3)	43.6(2)	2.665(7)	
	45.1(3)	4.823(6)	12.82(3)	43.0(2)	2.658(7)	
	46.9(6)	4.811(3)	12.78(3)	42.7(1)	2.656(6)	
	48.6(3)	4.798(1)	12.75(1)	42.34(6)	2.657(2)	
ssrl4/98	0.9(3)	5.031(3)	13.76(1)	50.27(7)	2.735(3)	Nonhydrostatic[b]
	21.1(2)	4.947(9)	13.43(4)	47.4(2)	2.715(9)	
	40.6(4)	4.892(9)	13.17(4)	45.5(2)	2.692(9)	
	44.3(4)	4.882(5)	13.11(2)	45.1(1)	2.685(5)	
	51.6(6)	4.861(7)	13.03(3)	44.4(1)	2.681(7)	
ssrl11/97	9.1(6)	4.993(4)	13.60(2)	48.94(9)	2.724(5)	Nonhydrostatic[b]
	27(4)	4.915(9)	13.41(4)	46.8(2)	2.728(9)	
	41(5)	4.88(1)	13.16(6)	45.2(2)	2.70(1)	
	0	5.049(5)	13.73(2)	50.5(1)	2.719(5)	Decompression
	0	5.0344(5)	13.7473(15)	50.29(1)	2.731(2)	Finger and Hazen 1980[c]

[a] With argon
[b] Without pressure medium
[c] With 4:1 methanol and ethanol

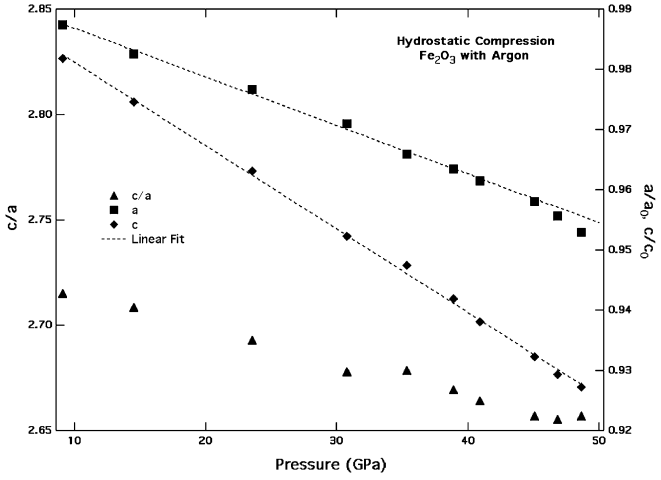

Fig. 3 Pressure dependence of the unit-cell parameters a/a_0 (*squares*) and c/c_0 (*diamonds*), with *subscript zero* indicating the zero-pressure value, and the ratio c/a (*triangles*) for α-Fe_2O_3 at room temperature. The *dashed lines* show linear fits to a/a_0 and c/c_0 vs. pressure

suggesting that the pressure derivative K_0' for α-Fe_2O_3 may be slightly larger than 4.0.

Detailed comparisons with other statically determined values (Bassett and Takahashi 1974; Wilburn and Bassett 1978; Sato and Akimoto 1979; Finger and Hazen 1980) are summarized in Table 2. Our modulus value, $K_0 = 206.1$ ($\pm$ 4.8) GPa using $K_0' = 4$, is close to Wilburn and Bassett's hydrostatically determined value, $K_0 = 199$ ($\pm$ 6) GPa (with $K_0' = 4$) obtained using a 4:1 methanol:ethanol solution as a pressure medium; it is 10% less than Bassett and Takahashi's nonhydrostatically determined value, $K_0 = 228$ GPa with $K_0' = 4$. These comparisons allow us to conclude that with argon as a medium, the pressure is quasihydrostatic over the entire pressure range of the present study.

The geometry of the diamond-anvil cell is such that the applied load can result in an anisotropic distribution of stress, even using a gasketed cell, with X-ray diffraction typically being sensitive to the strain nearly perpendicular to the applied load while the pressure measured by ruby fluorescence is related to the average stress, parallel and perpendicular to the applied load (Mao and Bell 1978; Kinsland and Bassett 1976; Jephcoat et al. 1986). Therefore, there can be a significant difference between the pressure ascribed to a diffraction pattern and the actual pressure acting on the sample. With nonhydrostatic compression, the normal stresses — and therefore the strains — perpendicular to the compression axis (which are those determined in the standard diffraction geometry) are less than the average pressure acting on the sample. This is the main reason for obtaining a large apparent value for K_0 from nonhydrostatic experiments. Although argon freezes at a pressure of about 1.2 GPa, it exhibits nearly hydrostatic behavior below 9.0 GPa (Mao et al. 1982). Our results suggest that the soft solid argon can provide an effectively hydrostatic environment to even higher pressure.

In more detail, we can analyze the linear compressibilities along the two unit-cell axes, a and c, according to the extended Eulerian finite-strain equation of state (Meade and Jeanloz 1990). The third-order Birch-Murnaghan equation of state along both a and c axes can then be expressed as:

$$F_i = K_{i0}[1 - 3/2(4 - K_{i0}')f_i] \ , \qquad (2)$$

where subscript $i = a$ and c, such that $f_a = 1/2[(a_0/a)^2 - 1]$ and $f_c = 1/2[(c_0/c)^2 - 1]$. In addition, K_{i0} is the linear incompressibility in the corresponding direction and the prime indicates pressure differentiation.

By fitting the data for a and c lattice parameters as a function of pressure, we can quantitatively determine the degree to which compression is isotropic. For a hexagonal unit cell, the linear incompressibilities along the unit cell axes are related by $1/K_0 = 2/K_{a0} + 1/K_{c0}$ (Nye 1985). Fitting the present data obtained with argon as a pressure medium, and assuming $K_{i0}' = 4$, yields $K_{a0} = 749.5$ (18.4) GPa and $K_{c0} = 455.7$ (21.4) GPa by a weighted fit to (2) (i.e., a weighted average of F_i). This shows that the c axis is approximately 1.6 times more compressible than the a axis.

The different incompressibilities along the a and c directions, and the change of c/a ratio as pressure increases, are due to changes in the atomic packing within the unit cell. Hematite has a corundum structure with space group D_{3d}^6 ($R\bar{3}c$). The basic geometry of this structure consists of hexagonal close-packed oxygen layers along the c axis, with Fe occupying two-thirds of the octahedral sites and O being surrounded by four Fe ions. The hexagonal unit cell is six oxygen layers high, and contains six formula units of Fe_2O_3. The different FeO_6 octahedral layers are linked to each other by a

Table 2 Isothermal bulk modulus of α-Fe_2O_3 at zero pressure

K_0 (GPa)	K_0'	Conditions	W A[b]	Reference
206.1 ± 4.8	4.0	w/argon, P < 50 GPa	Yes	This study
213.9 ± 13.6	4.0	w/argon, P < 50 GPa	No	This study
202.1 ± 3.8	4.3 ± 0.3	w/argon, P < 50 GPa	Yes	This study
213.3 ± 13.5	4.0 ± 0.1	w/argon, P < 50 GPa	No	This study
228	4.0	w/alcohol[a], P < 300 kbar		Bassett and Takahashi (1974)
196 ± 6	4.0	w/alcohol, P < 115 kbar		Wilburn and Bassett (1978)
231	4.0	w/alcohol, P < 30 kbar		Sato and Akimoto (1979)
178	4.0	w/alcohol, P > 30 kbar		Sato and Akimoto (1979)
225 ± 5	4.0	w/alcohol, P < 50 kbar		Finger and Hazen 1980
202.7	4.0	ultrasonic		Liebermann and Schreiber (1968)

[a] Alcohol – 4:1 methanol and ethanol
[b] WA – Weighted average

combination of vertex-, edge-, and face-sharing, which is complicated when compared with polyhedral linkages in many other structures but results in the high stability of the corundum structure of hematite (Wyckoff 1986). In detail, the FeO_6 octahedra in a given layer are linked to each other by sharing three edges, and those in different layers are linked by sharing faces. That is, each FeO_6 octahedron contains three shared and three unshared edges outside the basal plane, and one shared plus one unshared face in the basal and top planes.

In such a scheme, the O–O distance inside a sharing face is more difficult to compress than the O–O bonds involved in edge- or vertex-sharing. This suggests that the *a*-axis length should be more difficult to change than the *c* axis, since the sharing face planes are parallel the basal plane (i.e., perpendicular to the *c* axis). From projection on (1120) of part of the corundum structure (Megaw 1973), we can also conclude that the plane linked by pairs of FeO_6 octahedra which share faces has a higher atomic density, thus a weaker bonding energy between the planes along the direction perpendicular to this plane. This, in turn, leads to a greater decrease in the *c* axis than in the *a* axis under pressure, which results in the *c*/*a* ratio decreasing under pressure (i.e., the observed factor of 1.6 between the incompressibilities along the *a* and *c* axes).

Structure of the high-pressure phase at pressures above 50 GPa

In order to index the high-pressure phase, we calculated the diffraction patterns for the $GdFeO_3$ orthorhombic perovskite- and Rh_2O_3(II)-type structures (Liu 2000). The two calculated diffraction patterns look very similar, exhibiting only a small difference for low-intensity peaks at *d* spacings below 2.0 Å. Since the measured X-ray diffraction peaks become broadened at pressure, it is difficult to see such details in the experimental data, so it is hard to determine the structure of this high-pressure phase just by indexing the observed diffraction patterns.

To gain a better understanding of the high-pressure phase, we consider the effects of pressure on the various bond lengths. Because they share vertices, edges, and faces in the α-Fe_2O_3 unit cell, the FeO_6 octahedra must be irregular, and this is confirmed by the zero-pressure *c*/*a* ratio being much smaller (2.731 ± 0.002) than the value of 2.828 for the ideal corundum structure. The oxygen–oxygen distance of a shared edge is considerably shorter than that of an unshared edge, and the distance in the shared basal face is also considerably shorter than the corresponding distance in the unshared basal face. Similarly, the iron atoms are closer to the oxygen of the unshared faces than to the oxygen of the shared faces (Blake et al. 1966). Since the *c* axis is more compressible, the Fe–O–Fe angle along the *c* direction shrinks faster than that along the *a* direction, which leads to the FeO_6 octahedron exhibiting an increased degree of anisotropy along the *c* direction with increasing pressure. If they remain stable, the FeO_6 octahedra subsequently rotate and this may even lead to breaking of edge- or face-sharing bonds, inducing the observed structural transformation. Once this happens, one can expect a decreased degree of anisotropy, since now the FeO_6 octahedron is less distorted than before due to the breaking of shared bonds. Therefore, we conclude that the enhanced compressibility of the *c* axis may offer a structural reason for the high-pressure transformation, with (incipient) breaking of edge- or face-sharing bonds playing an important role.

Since more energy is required to break face-sharing bonds, shared-vertex or shared-edge bonds should break first with increasing pressure. Thus, if the α-Fe_2O_3 structure undergoes transformation at pressure, the first new structure is likely to contain shared faces with a decreased number of shared vertices or edges. Although both Rh_2O_3 (II) and $GdFeO_3$ perovskite structures have very similar X-ray diffraction patterns, their atomic packings are different. The Rh_2O_3 (II)-type structure contains pairs of RhO_6 octahedra which share faces, the same as corundum, but the number of shared edges in the Rh_2O_3(II)-type structure is decreased to two from three in the corundum structure (Shannon and Prewitt 1970). In contrast, the $GdFeO_3$ perovskite structure contains only vertex-sharing FeO_6 octahedra. Therefore, the sequence of high-pressure phase transitions of the α-Fe_2O_3 structure should be first to the Rh_2O_3 (II)-type structure, before going to the $GdFeO_3$ perovskite structure. This is consistent with predictions from first-principles calculations (Thomson et al. 1996).

From the above discussion, we index the high-pressure phase of α-Fe_2O_3 as the Rh_2O_3 (II)-type structure with a unit cell having lattice parameters $a = 6.6679(12)$ Å, $b = 4.6003(24)$ Å and $c = 4.9391(16)$ Å at 52.8 GPa. As seen in Fig. 4, the transformation is of first order, with a discontinuity in volume. At a pressure of 52.8 GPa, the low-pressure phase volume, $V_{LP} = 42.0$ Å^3 (estimated from the equation of state fit for the low-pressure phase) and the high-pressure phase volume, $V_{HP} = 37.9$ Å^3, yield a relative volume change of $(V_{LP}-V_{HP})/V_{LP} \approx 10\%$, in good agreement with the results of previous studies.

High-pressure transformation with laser heating

The high-pressure phase observed in α-Fe_2O_3 at about 50 GPa, identified as the Rh_2O_3 (II)-type structure, is related to the corundum structure by tilting of octahedra and breaking of nearest-neighbor bonds. High temperature may allow the sample to overcome kinetic barriers to alternative structures, thus allowing the corundum phase to transform at a lower pressure than without heating. We obtained the best diffraction pattern at 22 GPa after laser heating to a peak temperature of ~3500 K, shown in Fig. 5. Along with continuous laser heating, the use of a soft pressure medium results in a well-annealed sample and a significantly improved quality of diffraction pattern. It is clear that sharp new peaks appear after laser heating, which cannot be identified as other iron oxides or products from dissociation

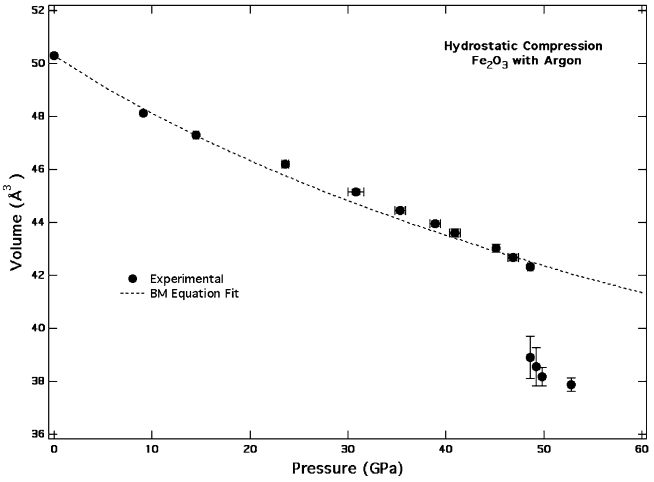

Fig. 4 Volume per formula unit of α-Fe_2O_3 as a function of pressure (SSRL3/99), showing the discontinuity around 50 GPa. The relative volume change across this transformation is about 10%. The *dashed line* indicates the fit of the low-pressure phase data to a second-order Birch–Murnaghan equation of state, with $K_0 = 206.1$ GPa and $K_0 = 4$

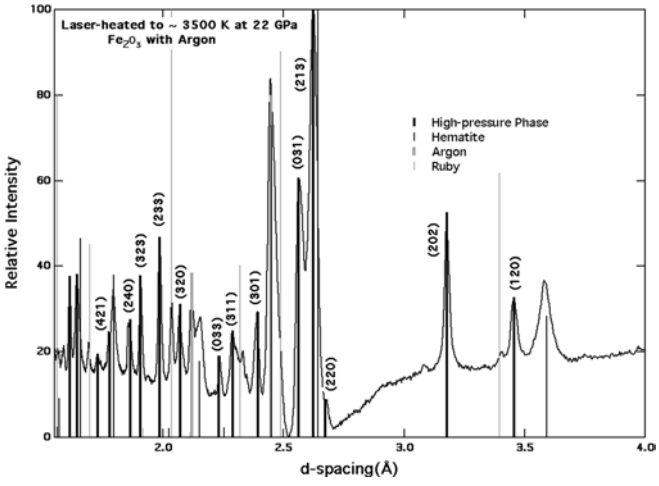

Fig. 5 X-ray diffraction pattern of α-Fe_2O_3 at 22 GPa, after heating to about 3500 K (SSRL4/98). *Thick black lines* indicate the diffraction peaks for the new high-pressure phase, and *thin black lines* are for hematite. The patterns of argon and ruby are shown with *thick and thin gray lines*, respectively. The high-pressure phase has been indexed as an orthorhombic structure with $a = 7.305(3)$ Å, $b = 7.850(3)$ Å and $c = 12.877(14)$ Å: *several Miller indices are labeled*

(i.e., Fe, FeO or Fe_3O_4), indicating that a phase transition has occurred by 22 GPa. This pressure is far lower than the phase transition observed from room-temperature (unheated) compression studies, as well as shock-wave measurements (~40–50 GPa).

Based on the two peaks at $d > 3.0$ Å, this new phase appears similar to the high-pressure phase above 50 GPa; but the diffraction pattern is more complicated and exhibits many new peaks for $d < 2.4$ Å. The present result is different from that obtained by Badro et al. (2002) from a sample laser-heated to 1500 K at 46 GPa: they report a X-ray diffraction pattern for the high-pressure phase similar to that obtained on cold compression to 60 GPa.

Analyzing the X-ray diffraction pattern suggests that our new high-pressure phase is orthorhombic, but not with the $GdFeO_3$- or Rh_2O_3 (II)-type structures. An indexing of the diffraction pattern yields lattice parameters of $a = 7.305(3)$ Å, $b = 7.850(3)$ Å and $c = 12.877(14)$ Å at 22 GPa (Table 3). There is currently no solution for the space group of this high-pressure phase, but the relatively large lattice parameters suggest a structure of lower symmetry that may be related (intermediate) to the high-pressure phase found by static compression without heating. There are still strong diffraction lines from hematite mixed with the diffraction pattern of this high-pressure phase. Therefore, in-situ high-pressure and temperature experiments are needed to further characterize this phase transition, and to check whether the sample totally or partially transforms to the high-pressure phase at 22 GPa during laser heating.

Table 3 Observed and calculated[a] *d*-spacings for the high-pressure phase of α-Fe_2O_3 at 22 GPa after laser heating to ~3500 K (SSRL4/98)

hkl	d_{obs} (Å)	d_{calc} (Å)	$(d_{obs} - d_{calc})/d_{calc}$
120	3.4561	3.4576	−0.0004
202	3.1789	3.1767	0.0007
220	2.6742	2.6738	0.0001
213	2.6222	2.6219	0.0001
031	2.5652	2.5644	0.0003
301	2.3906	2.3925	−0.0008
311	2.2886	2.2885	0.0000
033	2.2363	2.2343	0.0009
320	2.0700	2.0691	0.0004
233	1.9072	1.9060	0.0007
323	1.8616	1.8638	−0.0012
135	1.7770	1.7802	−0.0018
240	1.7289	1.7288	0.0000
421	1.6422	1.6422	0.0000
325	1.6128	1.6130	−0.0001

[a] With $a = 7.305(3)$ Å, $b = 7.850(3)$ Å, $c = 12.877(14)$ Å, and $V = 738.4$ Å^3

Conclusion

We compressed α-Fe_2O_3 statically up to 60 GPa. Fitting the X-ray diffraction data to the Birch–Munaghan equation of state yields a zero-pressure isothermal bulk modulus $K_0 = 206.1$ (± 4.8) GPa, assuming a pressure derivative $K_0 = 4.0$, which is in good agreement with the previously determined ultrasonic and hydrostatic-compression values. The more compressible *c* axis may induce the breaking of shared bonds in the order of vertex-sharing, edge-sharing, and then face-sharing. This in turn suggests that the high-pressure phase transition in α-Fe_2O_3 is from the corundum to the Rh_2O_3 (II) structures (possibly to be followed by transformation to the $GdFeO_3$ perovskite structure). The diffraction pattern after continuous laser heating reveals a new structural phase transformation of

α-Fe_2O_3 at 22 GPa, to an orthorhombic structure with $a = 7.305(3)$ Å, $b = 7.850(3)$ Å and $c = 12.877(14)$ Å at 22 GPa.

Acknowledgements We thank J. H. Ngyuen, K.-J. Kim, N. Funamori, A. Kavner, S. Akber, K. Lee, and H. Scott for help during this project, and SSRL staff for technical assistance. We also thank M.S.T. Bukowinski and M.P. Pasternak for helpful discussions. This work was supported by the National Science Foundation and University of California, and Stanford Synchrotron Radiation Laboratory is funded by the Department of Energy.

References

Badro J, Fiquet G, Struzhkin VV, Somayazulu M, Mao HK, Shen G, Le Bihan T (2002) Nature of the high-pressure transition in Fe_2O_3 hematite. Phys Rev Lett 89: 5504–1–4

Bassett WA, Takahashi T (1974) X-ray diffraction studies up to 300 kbars. In: Wentorf RH Jr (ed) Advances in high-pressure research. Academic Press, New York, pp 165–247

Birch F (1978) Finite strain isotherm and velocities for single-crystal and polycrystalline NaCl at high pressure and 300 K. J Geophys Res 83: 1257–1268

Blake RL, Hessevick RE, Zoltai T, Finger LW (1966) Refinement of the hematite structure. Am Mineral 51: 123–129

Cynn H, Isaak DG, Cohen RE, Nicol MF, Anderson OL (1990) A high-pressure phase transition of corundum predicted by the potential induced breathing model. Am Mineral 75: 439–442

Finger LW, Hazen RM (1980) Crystal structure and isothermal compression of Fe_2O_3, Cr_2O_3, V_2O_3, up to 50 kbars. J Appl Phys 51: 55362–5367

Funamori N, Jeanloz R (1997) High-pressure transformation of Al_2O_3. Science 278: 1109–1111

Heinz DL, Jeanloz R (1987) Temperature measurements in the laser-heated diamond cell. In: Manghnani MH, Syono Y (eds) High-pressure research in mineral physics. American Geophysical Union, Washington DC, pp 113–127

Jeanloz R (1989) Shock wave equation of state and finite strain theory. J Geophys Res 94: 5873–5886

Jeanloz R, Heinz DL (1984) Experiments at high temperature and pressure: laser heating through the diamond cell. J Phys (Paris) 45: 83–92

Jeanloz R, Kavner A (1996) Melting criteria and imaging spectroradiometry in laser-heated diamond-cell experiments. Phil Trans Roy Soc London A 354: 1279–1305

Jephcoat AP, Mao HK, Bell PM (1986) Static compression of iron to 78 GPa with rare gas solids as pressure-transmitting media. J Geophys Res 91: 4677–4684

Kinsland GL, Bassett WA (1976) Modification of the diamond cell for measuring strain and strength of materials at pressures up to 300 kbar. Rev Sci Instrum 47: 130–133

Knittle E, Jeanloz R (1986) High-pressure electrical resistivity measurements of Fe_2O_3 : Comparison of static-compression and shock-wave experiments to 61 GPa. Solid State Commun 58: 129–131

Liebermann RC, Schreiber E (1968) Elastic constants of polycrystalline hematite as a function of pressure to 3 kilobars. J Geophys Res 73: 6585–6590

Liu H (2000) Synchrotron radiation X-ray diffraction study of high- pressure phase transformations in Fe_2O_3. PhD Thesis, Jilin University, Changchun, China

Mao HK, Bell PM (1978) Design and varieties of the megabar cell. Year Book Carnegie Institute of Washington 77: 904–913

Mao HK, Mao R, Bell PM (1982) In: Backman CM, Johannisson T, Tegner L (eds) Abstracts of the 8th AIRAPT Conference Uppsala. ISBN, Sweden, vol. II, pp 453

Marton FC, Cohen RE (1994) Prediction of a high-pressure phase transition in Al_2O_3. Am Mineral 79: 789–792

McQueen RG, Marsh SP (1966) In: Clark SP Jr (ed) Handbook of physical constants. Geol Soc Am Mem 97, New York, pp 153

Meade C, Jeanloz R (1990) Static compression of $Ca(OH)_2$ at room temperature: Observations of amorphization and equation of state measurements to 10.7 GPa. Geophys Res Lett 17: 1157–1160

Megaw HD (1973) Crystal structures: a working approach. Saunders, London, pp 229

Nguyen JH, Jeanloz (1993) A computer program to analyze X-ray diffraction films. Rev Sci Instrum 64: 3456–3461

Nye JF (1985) Physical properties of crystals. Oxford University Press, UK pp 329

Olsen JS, Cousins CSG, Gerward L, Jhans H, Sheldon BJ (1991) A study of the crystal structure of Fe_2O_3 in the high pressure range up to 65 GPa using synchrotron radiation. Physica Scripta 43: 327–330

Pasternak MP, Rozenberg GK, Machavariani GY, Naaman O, Taylor RD, Jeanloz R (1999) Breakdown of the Mott–Hubbard state in Fe_2O_3: a first-order insulator-metal transition with collapse of magnetism at 50 GPa. Phys Rev Lett 82: 4663–4666

Reid AF, Ringwood AE (1969) High-pressure scandium oxide and its place in the molar volume relationships of dense structure of M_2X_3 and ABX_3 type. J Geophys Res 74: 3238–3252

Ross M, Mao HK, Bell PM, Xu JA (1986) The equation of state of dense argon: a comparison of shock and static studies. J Chem Phys 85: 1028–1033

Rozenberg GK, Dubrovinsky LS, Pasternak MP, Naaman O, Bihan TL, Ahuja R (2002) High-pressure structural study of hematite Fe_2O_3. Phys Rev (B) 65: U122–U129

Sato R, Akimoto S (1979) Hydrostatic compression of four corundum-type compounds: α-Al_2O_3, V_2O_3, Cr_2O_3, α-Fe_2O_3. J Appl Phys 50: 5285–5291

Shannon RD, Prewitt CT (1970) Synthesis and structure of a new high-pressure form of Rh_2O_3. J Solid State Chem 2: 134–136

Suzuki T, Yagi T, Akimoto S, Ito A, Morimoto S, Syono Y (1985) X-ray diffraction and Mossbauer spectrum on the high pressure phase of Fe_2O_3. In: Minomura S (ed) Solid state physics under pressure. Terra Scientific Tokyo, Japan pp 149–154

Syono Y, Ito A, Morimoto S, Suzuki T, Yagi T, Akimoto S (1984) Mossbauer study on the high pressure phase of Fe_2O_3. Solid State Commun 50: 97–100

Thomson KT, Wentzcovitch RM, Bukowinski MST (1996) Polymorphs of alumina predicted by first principle: putting pressure on the ruby pressure scale. Science 274: 1880–1882

Yagi T, Akimoto S (1982) Rapid X-ray measurements to 100 GPa range and static compression of α-Fe_2O_3. In: Akimoto S, Manghnani MH (eds) High-pressure research in geophysics. Center Acad Publ Japan, Tokyo, pp 81–90

Wilburn DR, Bassett WA (1978) X-ray diffraction compression studies of hematite under hydrostatic, isothermal conditions. J Geophys Res 83: 3509–3512

Wyckoff RWG (1986) Crystal structures, vol 2. Krieger, Malabar, Florida, pp 7–8